Volume 17
Number 10
October 1978

Inorganic Chemistry

Contribution from the Department of Chemistry,
University of Virginia, Charlottesville, Virginia 22901

Absorption and Magnetic Circular Dichroism Spectra of Hexafluoroosmate(IV) and Hexafluoroiridate(IV) in the Cubic Host Cs_2GeF_6

L. C. WEISS,[1] P. J. McCARTHY, J. P. JASINSKI, and P. N. SCHATZ*

Received March 6, 1978

Ligand field (d–d) transitions of Os^{4+} and Ir^{4+} doped into the cubic host, Cs_2GeF_6, have been studied at low temperatures using absorption and magnetic circular dichroism (MCD) spectroscopy. OsF_6^{2-} shows many sharp, well-defined lines permitting a detailed interpretation of the interconfigurational d–d bands. (The crystal was too dilute for observation of the intraconfigurational bands.) Two intense a_{1g} progressions dominate the spectrum and have been assigned as A_{1g} ($^3T_{1g}$ (t_{2g}^4)) → T_{1g} ($^3T_{1g}$ ($t_{2g}^3e_g$)) and T_{1g} ($^3A_{1g}$ ($t_{2g}^3e_g$)). Examination of the weaker lines within these two progressions shows that transitions to T_{2g} states are generally less intense than those to T_{1g} states. No transitions to A_{1g}, A_{2g}, or E_g states are observed. The assigned states in OsF_6^{2-} are fit well by the parameters B = 625 cm^{-1}, C = 2969 cm^{-1}, Dq = 2450 cm^{-1}, and ζ = 2800 cm^{-1}. For IrF_6^{2-}, intraconfigurational transitions within the spin–orbit split $^2T_{2g}$ (t_{2g}^5) ground state are observed in addition to the interconfigurational transitions. The latter are not as well resolved as in OsF_6^{2-}, and a less detailed interpretation has been possible. However, four excited states are assigned which are fit well by the ligand field parameters B = 641 cm^{-1}, C = 3140 cm^{-1}, Dq = 2450 cm^{-1}, and ζ = 3500 cm^{-1}.

I. Introduction

The d–d spectra of second- and third-row transition-metal ions have been much less studied than those of the first transition series, and the ligand field parameters are generally not well-known. Accordingly, studies of the electronic spectra of the hexafluoro anions of the 4d and 5d series are of particular interest because the fluoride ligand occupies a low position in the spectrochemical series and has a very high optical electronegativity. As a result, the d–d transitions occur at somewhat lower energies than do those of many other ligands, and at the same time, the ligand-to-metal charge-transfer transitions are shifted to considerably higher energy. Both of these effects facilitate the observation of the d–d bands.

This paper reports a study of the electronic spectra of two 5d transition-metal hexafluoro anions, OsF_6^{2-} and IrF_6^{2-}. Magnetic circular dichroism (MCD)[2] as well as electronic absorption spectra have been utilized in the analysis of the crystal field transitions. MCD lends itself particularly well to the interpretation. This technique has previously been shown to be very useful in the interpretation of the charge-transfer transitions of the corresponding complexes, OsX_6^{2-} and IrX_6^{2-} (X = Cl or Br),[3-7] as well as for the OsI_6^{2-} species and some trans-mixed hexahalo complexes of Os^{4+} and Ir^{4+}.[8] We refer to the literature for further details of the technique.[2]

We shall use ligand field theory as our model since MO theory is still of limited predictive value[9,10] for the systems under consideration. Our ligand field bases will be "complete" so that the use of strong or weak field programs is strictly a matter of convenience, and comparisons of eigenvalues between the two provide a very useful numerical check. In our analysis we shall also in general ignore the possibility that "solid-state effects" occur as a consequence of phonon coupling throughout the Brillouin zone. Thus we will make the k = 0 assumption, and so the host lattice is assumed to provide an octahedral field and otherwise manifests itself only through low-energy sidebands built on magnetic dipole origins. This simplest approach permits plausible interpretation of virtually all observed features.

In octahedral systems, d–d electric dipole transitions are parity-forbidden and gain intensity chiefly through the coupling of the gerade excited state, $\Gamma_g\gamma$, with an appropriate ungerade vibration ν_i, of the molecular ion (where i = normal mode of vibration $\nu_3(t_{1u})$, $\nu_4(t_{1u})$, or $\nu_6(t_{2u})$). In effect, such coupling mixes other electric dipole allowed (ungerade) states, $\Gamma_u'\gamma'$, with the electric dipole forbidden (gerade) excited state, $\Gamma_g\gamma$. The application of vibronic analysis to MCD spectroscopy has previously been discussed in detail.[11,13]

II. Experimental Section

Crystal Growth. It was found that transparent crystals of Cs_2GeF_6 could be grown from 6 M HF solutions. The appropriate dopant and the Cs_2GeF_6 host were dissolved in a small volume of 6 M HF in a 50-mL polypropylene beaker over a hot plate. The beaker was placed in a Nalgene desiccator over concentrated sulfuric acid in the presence of a beaker of solid KOH, and the desiccator was then sealed and set aside for a period of several weeks to allow "evaporation" to occur. This solution growth method produced crystals of good optical quality although it offered very limited control over dopant concentrations. The crystals required little polishing and produced no depolarization of circularly polarized light at low temperature. (Depolarization checks were made by measuring the known circular dichroism of a naturally optically active solution *after* the light beam had passed through the low-temperature crystal.)

The crystal of Cs_2GeF_6:Os^{4+} was grown using H_2OsCl_6 as the dopant. One to two drops of the liquid were added to a solution of 0.9 g of Cs_2GeF_6 in about 15 mL of 6 M HF. Crystals of Cs_2GeF_6:Ir^{4+} were grown using Cs_2IrF_6. This dopant was very kindly supplied by Professor Wilhelm Preetz, having been prepared by reaction of Cs_2IrCl_6 with $CsHF_2$ at temperatures of 300–400 °C.[12] Continuous ionophoresis was required to remove traces of Cs_2IrCl_6.[12] In growing the crystals of Cs_2GeF_6:Ir^{4+}, 0.0406 g of Cs_2IrF_6 and 0.5265 g of Cs_2GeF_6 were dissolved in approximately 25 mL of 6 M HF and set aside to evaporate. A higher mole percent (5.7) of Cs_2IrF_6 was put into solution than was obtained in the crystal used for analysis (~2.4).

Magnetooptical Techniques. Two different cryostats were used, both manufactured by The Oxford Instrument Co. Ltd. One has been

0020-1669/78/1317-2689$01.00/0

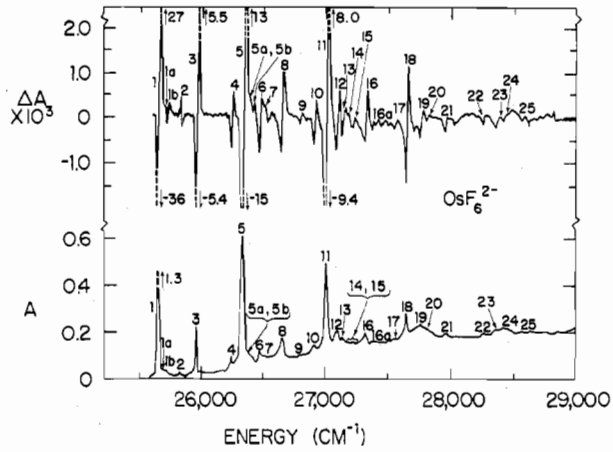

Figure 1. Absorption spectrum (A = absorbance) and MCD [$\Delta A = (A_L - A_R)$ per tesla] for the lower energy region of Cs_2GeF_6:Os^{4+} at ~10 K. Multiplication by 1400 converts A to ϵ (molar extinction coefficient). The amplitude is indicated for each feature which is off scale.

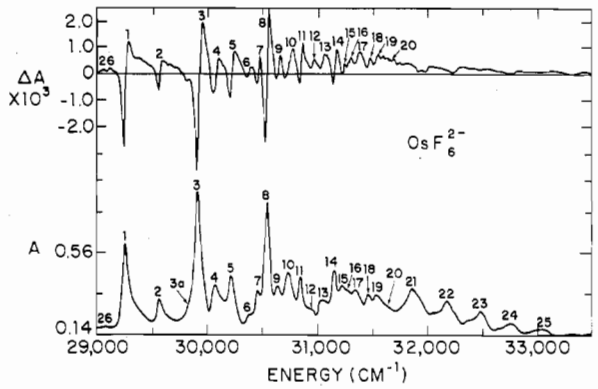

Figure 2. Absorption (A) and MCD (ΔA) spectrum for the higher energy region of Cs_2GeF_6:Os^{4+} at ~10 K. Notation and conversion factors are as in Figure 1.

described previously.[13] It afforded operating fields as high as 7.2 T but had relatively poor temperature control and could not give sample temperatures below ~10 K.

The second system provided excellent temperature control over a wide range (1.5–300 K). It was a Spectro Mag-SM4 consisting of a superconductive split pair mounted with field direction horizontal in the rectangular tail of a liquid helium cryostat. Crystals were loaded from the top of the cryostat into an exchange gas cell at the center of the magnet (i.e., crystals were not under vacuum). Temperatures in the range 1.5–4.2 K were achieved by filling the exchange gas cell with liquid helium thus immersing the crystal; the helium vapor pressure was then reduced by pumping. Temperatures ≥4.2 K were obtained by filling with exchange gas and varying the helium flow rate, with an electrical heater providing fine control. The temperature was monitored with a carbon resistor attached to the sample holder. A normal operating field of 5.0 T was used, although the system had 6.0 T capability.

MCD and absorption spectra were recorded in the range 19 000–33 000 cm^{-1} using a 450-W xenon arc lamp and either a Spex 1400-II $^3/_4$-m double grating monochromator which provided spectral slit widths approaching 1 cm^{-1} or a Durrum-Jasco. The range, 33 000–40 000 cm^{-1}, was examined with the Durrum-Jasco J-10B CD spectrophotometer (double prism) using the same light source. Infrared MCD data were recorded using a high-intensity tungsten–halogen light source, a Spex 1670 Minimate equipped with an infrared grating blazed at 2 μ (300 lines/mm), a Morvue modulator, and lead selenide detector. All IrF_6^{2-} absorption data were recorded with a Cary 14. Resolution of MCD data in the infrared was poor (~100 cm^{-1}), but in all other cases the spectral slit width was sufficiently narrow to permit true line shapes to be recorded.

Dopant Concentrations and Oscillator Strengths. The concentrations of dopants in the crystals were determined by neutron activation analysis and for the data in Figures 1–7 were, for Os^{4+}, ~0.011 M = 0.12 mol % and, for Ir^{4+}, ~0.22 M = 2.4 mol %. These concentrations are only reliable to a factor of about 2 in view of the smallness of the crystals (~10–25 mg, ~0.1 cm thick). ϵ values are calculated from these concentrations assuming a uniform absorption cross section. For Os^{4+}, the oscillator strengths (f) of the various integrated absorption lines fell in the range 5×10^{-6} to 2×10^{-4} confirming the d–d character of the observed transitions ($f \simeq 4.32 \times 10^{-9} \int \epsilon \, d\nu$). The Ir^{4+} crystals showed ϵ_{max} values for the fairly broad (interconfigurational) lines in the range ~10–50, and oscillator strengths of the broad collective bands centered at about 25 800 cm^{-1} and at about 32 500 cm^{-1} were found to be ~4.8×10^{-6} and 2.5×10^{-5}, respectively, again providing strong evidence of the ligand field nature of the spectra.

III. Results and Discussion

A. OsF_6^{2-}. The overall absorption and MCD spectra are shown in Figures 1 and 2. The host, Cs_2GeF_6, is cubic, space group O_h^5.[14] The Ge^{4+} site symmetry is O_h, and analysis of the spectrum has been carried out assuming O_h site symmetry for Os^{4+} as well. The effect of a small tetragonal distortion is seen in a splitting of the first spectral line, and this will be discussed later. No such effects are observed elsewhere.

Electronegativity considerations predict that the ligand-to-metal charge-transfer transitions of transition-metal hexafluorides should occur at considerably higher energies than those for the other hexahalides, and the interconfigurational d–d transitions should thereby be revealed. Accordingly, the diffuse reflectance spectrum of K_2OsF_6 in the energy region 10 000–45 000 cm^{-1} has been assigned by Allen et al.[9,15] to the intraconfigurational ($t_{2g}^4 \rightarrow t_{2g}^4$) and "spin-allowed" interconfigurational ($t_{2g}^4 \rightarrow t_{2g}^3 e_g$) d–d transitions of OsF_6^{2-}. Fairly weak, intraconfigurational bands occurred at 12 700, 18 500, and 22 500 cm^{-1}, and the stronger, interconfigurational absorptions appeared at 30 000 cm^{-1} (broad) and at 42 000 cm^{-1}. Weaker bonds were observed at 5600 and 3200 cm^{-1} (hexachlorobutadiene mull data) and were also assigned as intraconfigurational d–d bands, specifically, those occurring within the spin–orbit split ground term. Our low-temperature MCD and absorption spectra cover the energy region 25 500–34 000 cm^{-1} and consist of sharp, well-defined lines as opposed to the broad, unresolved diffuse reflectance bands. More dilute crystals will be required to study the much more intense transitions to higher energy, and none of the weaker, intraconfigurational d–d bands were observed since we were unable to introduce the required higher concentration of dopant into the host.

The ground state of the low-spin $5d^4$ Os^{4+} ion in an O_h field is the A_{1g} spin–orbit component of the $^3T_{1g}(t_{2g}^4)$ term.[17b] The spectrum of OsF_6^{2-} in the region of study is dominated by two intense a_{1g} progressions which we shall show correspond to transitions from the A_{1g} ground state to two T_{1g} excited states ($t_{2g}^3 e_g$). The MCD[16] is characterized by a series of $\mathcal{A}$ terms[16] (no $\mathcal{C}$ terms[16] are observed since the ground state of Os^{4+} is nondegenerate). No transitions to A_{1g}, A_{2g}, or E_g states are observed (i.e., absorption bands without accompanying MCD $\mathcal{A}$ terms), reinforcing arguments[17] that these transitions should be weaker than those to T_{1g} and T_{2g} states. However, it is found that transitions to T_{1g} states are, in general, more intense than transitions to T_{2g} states, contrary to prediction.[17] The first progression lies in the energy region from 25 500 to 29 000 cm^{-1}.

1. 25 500-29 000-cm^{-1} Region of OsF_6^{2-} (Figure 1). We shall first show that the intense progression in this region may with confidence be assigned to A_{1g} ($^3T_{1g}$) $\rightarrow$ $T_{1g}^{(1)}$ ($^3T_{1g}$), where $T_{1g}^{(1)}$ is the lowest lying state of the $t_{2g}^3 e_g$ excited configuration. (A superscript in parentheses differentiates between states of the same symmetry coming from the same term—$^3T_{1g}$ in this case. Throughout, a single term and/or configuration associated with a state designates the single most important contributor.)

Table I. Ground- and Excited-State Vibrational Frequencies (cm^{-1}) of OsF_6^{2-}

$\nu_1(a_{1g})$	$\nu_3(t_{1u})$	$\nu_4(t_{1u})$	$\nu_6(t_{2u})$	$\nu_7(t_{1u})$
690[a]	548[b]	262[c]	185[a]	118[c]
660[d]	595[a]	320[a]		~75[a]
	555[d]	305[d]		

[a] Excited-state frequency from assignment of lines 1, 1a, 1b, 2, 3, 4, and 5 (Figure 1). [b] Ground-state frequency from J. R. Ferraro, "Low-Frequency Vibrations of Inorganic and Coordination Compounds", Plenum Press, New York, N.Y., 1971, pp 118 and 119. [c] Ground-state frequency from D. M. Adams and H. A. Gebbie, *Spectrochim. Acta*, 19, 925 (1963). [d] Excited-state frequency from assignment of lines 1, 2, 3a, and 3 (Figure 2).

Table II. Calculated Properties of Low-Lying Interconfigurational T_{1g} and T_{2g} Excited States of OsF_6^{2-}

excited state $(t_{2g}^3e_g)$[a]	energy,[b] cm^{-1}	magnetic moment[b,c]	transition moment[b,c] $(A_1 \rightarrow T_1)$
$T_{1g}^{(1)}(^3T_{1g})$	25 560	0.407	2.128
$T_{1g}^{(2)}(^3T_{1g})$	26 678	−0.552	0.134
$T_{2g}(^3E_g^{(1)})$	27 429	−0.786	
$T_{1g}(^3T_{2g})$	28 054	−0.353	−0.051
$T_{2g}(^3T_{1g})$	28 862	0.021	
$T_{2g}(^3T_{2g})$	29 340	0.391	
$T_{1g}(^3A_{1g})$	29 864	1.249	0.171
$T_{2g}(^3A_{2g})$	29 909	1.842	
$T_{2g}(^3E_g^{(2)})$	31 831	−1.384	
$T_{1g}(^3E_g^{(2)})$	32 275	−0.660	0.113
$T_{2g}(^1T_{2g})$	35 223	−0.186	

[a] Superscripts (1) and (2) differentiate between states of the same symmetry coming from the same term and also between terms having the same term symbol. The term in parentheses designates the single most important contributor to the state. [b] Using the parameters (in cm^{-1}) $B = 625$, $C = 2969$, $Dq = 2450$, and $\zeta = 2800$. [c] In Bohr magnetons (β) for the operator $(L_z + 2S_z)$. The intensity of the transition is proportional to the absolute square of the magnetic dipole transition moment, and the dipole strength is given by $D(\beta^2) = 1/d_a \Sigma_{a\rightarrow j} |\langle j|(-\beta/\hbar)\cdot(\vec{L} + 2\vec{S})|a\rangle|^2 = 106.84 \int (\epsilon/\nu)\, d\nu$. The magnitude of the $\mathcal{A}$ term is directly proportional to the magnetic moment of the excited state. The peak-to-trough amplitude varies as the inverse second power of the line width.

The observed pattern up to the first repeat in the a_{1g} progression consists principally of four lines whose respective MCD shows a large positive $\mathcal{A}$ term (line 1), a small negative $\mathcal{A}$ term (line 2), and two larger positive $\mathcal{A}$ terms (lines 3 and 4). One must assume that these lines are all associated with the same excited state since the energy separation of the two lowest $t_{2g}^3e_g$ states is much larger than 600–700 cm^{-1} no matter how the parameters are varied in a ligand field calculation. Bearing these points in mind, a combination of arguments leads to a unique assignment. First, a four-line pattern suggests a T_{1g} rather than a T_{2g} excited state since the former may have a magnetic dipole allowed origin with up to three prominent electric dipole allowed vibronic sidebands (corresponding to the three ungerade octahedral vibrations, $\nu_3(t_{1u})$, $\nu_4(t_{1u})$, and $\nu_6(t_{2u})$). In contrast, the origin is forbidden for a T_{2g} excited state. Tentatively assigning line 1 as a magnetic dipole origin, we note that the spacings of lines 1–4 are reasonable in comparison with known ground-state ν_3 and ν_4 vibrational frequencies (Table I) if we associate lines 2–4, respectively, with ν_6, ν_4, and ν_3.

Let us now examine the MCD patterns. Faraday parameters have been calculated[18] using Griffith's irreducible tensor method[19] and its extension to the O^* double group by Dobosh.[20,21] Required magnetic moments and magnetic transition moments (Table II) were respectively calculated using "complete" strong- and weak-field bases; the latter is well suited for transition moment calculations. (Agreement of eigenvalues between the two bases also serves as a numerical check of both calculations.) The Faraday calculations are summarized in Tables III and IV. We note (Table III) that a T_{1g} origin and associated t_{1u} vibronic line must have an $\mathcal{A}$ term of the same sign and opposite that of the associated t_{2u} vibronic line, consistent with our assignments. Furthermore, the T_{1g} magnetic moment must be positive to account for the observed absolute signs. Again this is consistent (Table II) with our assignment of the origin to $T_{1g}^{(1)}$. In addition, Table II predicts that the magnetic dipole transition, $A_{1g} \rightarrow T_{1g}^{(1)}$, should be at least *two orders of magnitude* more intense than any other magnetic dipole line in the region. In fact, the experimentally observed dipole strength of line 1 is $\sim 45\beta^2$ compared to a predicted value (Table II) of $13.6\beta^2$ (β = Bohr magneton). While the agreement is only rough, any of the other magnetic dipole transitions would be far too weak to account for line 1.

Finally, lines 1 and 3 are sufficiently isolated to permit extraction of reliable Faraday and absorption parameters. These are found to agree quite well (Table IV) with the parameters calculated on the basis of the proposed assignment.

Thus we believe that the assignment of line 1 has been established beyond a reasonable doubt, and this assignment will be the foundation for all of our subsequent analysis. Closer examination reveals a splitting of line 1 which will be discussed in some detail later. Lines 1a and 1b are attributed to lattice vibrations.

The a_{1g} progression $(n\nu_1(a_{1g}) + 1\nu(\gamma_u)$, $\gamma_u = t_{1u}, t_{2u})$ for the $A_{1g}(^3T_{1g}) \rightarrow T_{1g}^{(1)}(^3T_{1g})$ transition is reasonably long, n = 0, 1, 2, and 3 being definitely observed, and assignments of the lines are summarized in Table V. The $n = 0$ lines are most intense, so the no-phonon energy is taken as the equilibrium vertical excitation of the transition. The 690-cm^{-1} value for $\nu_1(a_{1g})$ is observed to decrease from $n = 0$ to $n = 1$, etc., indicating anharmonicity in the excited state.

In carrying out crystal field calculations, it was observed that the order of those states having nonzero magnetic moments (i.e., "MCD-active" states) did not change as parameters were varied widely. This order has therefore been

Table III. Faraday Parameters for Magnetic Dipole and Vibronic[a] Transitions of OsF_6^{2-}

A	J	N	j	$\mathcal{A}_1/\mathcal{D}_0$[c]
A_{1g}	T_{1g}[b]			$2E$
A_{1g}	T_{1g}	T_{1u}	t_{1u}	E
A_{1g}	T_{1g}	T_{1u}	t_{2u}	$-E$
A_{1g}	T_{2g}	T_{1u}	t_{1u}	$-F$
A_{1g}	T_{2g}	T_{1u}	t_{2u}	F

[a] For both ground-state and excited-state mixing. [b] Magnetic dipole transition. [c] Where $\langle T_1 1|L_z + 2S_z|T_1 1\rangle = E$ and $\langle T_2 1|L_z + 2S_z|T_2 1\rangle = F$, and where A is the ground state, J is the excited state, N refers to the mixing state, and j is the allowing vibration.

Table IV. Observed and Calcualted Faraday Parameters[a]

line no.	progression	$\mathcal{A}_1/\mathcal{D}_0$ obsd	$\mathcal{A}_1/\mathcal{D}_0$ calcd	$\mathcal{B}_0/\mathcal{D}_0$ obsd	$\mathcal{B}_0/\mathcal{D}_0$ calcd
1	I	+1.10	+0.82	−0.00134	−0.00084[b]
3	I	+0.54	+0.40		
6 and 7	I	+0.24	+0.14		
12, 13, and 14	I	+0.56	+0.94		
1	II	+0.86	+2.50	−0.0118	−0.0174

[a] The observed parameters are obtained by moment analysis.[2] [b] Assuming mixing of ground state with the lowest (2857 cm^{-1}) T_{1g} state only. The next T_{1g} state is at ~13 000 cm^{-1}. Excited-state mixing with all T_{1g} states within 7000 cm^{-1} of $T_{1g}^{(1)}$ is included. Mixing states of other than T_{1g} symmetry make no contribution.

Table V. Assignment of 25 500–29 000 cm^{-1} Region of OsF_6^{2-} (Figure 1)[a]

line no.	sign of $\mathcal{A}$ term	obsd energy, cm^{-1}	calcd energy, cm^{-1} (from Table II)	excited state $(t_{2g}{}^3e_g)$[b]
I	+	25 655	25 560	$T_{1g}{}^{(1)}({}^3T_{1g})$
1a	−	25 720[c]		line 1 + ?[c]
1b	+	25 730[c]		line 1 + $\nu_7(t_{1u})$[c]
2	−	25 840		line 1 + $\nu_6(t_{2u})$
3	+	25 975		line 1 + $\nu_4(t_{1u})$
4	+	26 250		line 1 + $\nu_3(t_{1u})$
5	+	26 345		line 1 + $\nu_1(a_{1g})$
5a	−	26 410[c]		line 1 + ? + ν_1[c]
5b	+	26 420[c]		line 1 + $\nu_7 + \nu_1$[c]
6	+	26 475	26 678	$T_{1g}{}^{(2)}({}^3T_{1g}) + \nu_6$
7	−	26 520		line 1 + $\nu_6 + \nu_1$
8	+	26 655		line 1 + $\nu_4 + \nu_1$
9	+	26 795		?
10	+	26 915		line 1 + $\nu_3 + \nu_1$
11	+	27 010		line 1 + $2\nu_1$
12	+	27 100	27 429	$T_{2g}({}^3E_g{}^{(1)}) + \nu_4$
13	+	27 140		line 6 + ν_1
14	−	27 195		line 1 + $\nu_6 + 2\nu_1$
15	+	27 225		?
16	+	27 325		line 1 + $\nu_4 + 2\nu_1$
16a	+	27 375		$T_{2g}({}^3E_g{}^{(1)}) + \nu_3$
17	+	27 565		line 1 + $\nu_3 + 2\nu_1$
18	+	27 650		line 1 + $3\nu_1$
19	+	27 770		line 6 + $2\nu_1$
20	+	27 815		?
21	+	27 970		line 1 + $\nu_4 + 3\nu_1$
22	+	28 265		line 1 + $4\nu_1$
23	+	28 380		line 6 + $3\nu_1$
24	+	28 435	28 054	$T_{1g}({}^3T_{2g}) + \nu_6$
25	+	28 585		line 1 + $\nu_4 + 4\nu_1$
26[d]	+	29 100		line 24 + ν_1

[a] No vibrational modes of $OsCl_6^{2-}$ are observed anywhere in the spectrum indicating the absence of this impurity. [b] Superscripts (1) and (2) differentiate between states of the same symmetry coming from the same term and also between terms having the same term symbol. [c] Lattice modes. [d] See Figure 2.

used as a guide in assigning other states which underlie the more intense progression. Of the still unassigned lines, 6 and 12 are most intense, both showing positive $\mathcal{A}$ terms. Ligand field calculations indicate that three excited $(t_{2g}{}^3e_g)$ states, $T_{1g}{}^{(2)}$ $({}^3T_{1g})$, T_{2g} $({}^3E_g{}^{(1)})$, and T_{1g} $({}^3T_{2g})$, are in the appropriate energy region. Accordingly, line 6 has been assigned to the transition A_{1g} $({}^3T_{1g}) \rightarrow T_{1g}{}^{(2)}$ $({}^3T_{1g})$, this excited state being the lowest of the three. The sign of the magnetic moment of this state (Table II) further requires that line 6 be the $\nu_6(t_{2u})$ vibronic sideband (Tables III and IV). None of the other lines that one might expect for this transition are observed. The magnetic dipole origin is predicted (Table II) to be ~250 times weaker than line 1 and could indeed lie under line 5. The t_{1u} sidebands are evidently weaker than those for t_{2u} in this case, a situation which is not unusual.[5-7,22-24] In order to further confirm the assignment of line 6, moment analysis was carried out over the two overlapping lines, 6 and 7. Reasonable agreement between observed and calculated $\mathcal{A}_1/\mathcal{D}_0$ values is obtained (Table IV). Lines 13, 19, and 23 appear to be a_{1g} repeats of line 6, $\nu_1(a_{1g}) \simeq 665$ cm^{-1}.

According to ligand field calculations, the T_{2g} $({}^3E_g{}^{(1)})$ state is next in energy, lying about 750 cm^{-1} away from $T_{1g}{}^{(2)}$ $({}^3T_{1g})$. Turning to the remaining unassigned lines, 12 is the most intense and lies at an energy appropriate for assignment to A_{1g} $({}^3T_{1g}) \rightarrow T_{2g}$ $({}^3E_g{}^{(1)})$. In that case, the sign of the magnetic moment (Table II) requires assignment to either $A_{1g} \rightarrow T_{2g} + \nu_4$ or $A_{1g} \rightarrow T_{2g} + \nu_3$. Since the former is generally more intense, line 12 is assigned as $A_{1g} \rightarrow T_{2g} + \nu_4$ and the much weaker line 16a (275 cm^{-1} away) is assigned as $A_{1g} \rightarrow T_{2g} + \nu_3$. A moment analysis for the overlapping lines 12–14 on the basis of this and previous assignments gives a reasonable $\mathcal{A}_1/\mathcal{D}_0$ value (Table IV) considering the baseline uncertainties in the absorption spectrum. No line due to $\nu_6(t_{2u})$ is observed, and no a_{1g} repeats of lines 12 and 16a appear suggesting that the ground- and excited-state potential surfaces are almost identical.

The state next in energy, T_{1g} $({}^3T_{2g})$, is predicted by all ligand field calculations to lie 600–700 cm^{-1} higher, and its magnetic moment is negative (Table II), indicating that only one positive $\mathcal{A}$ term would be observed $(A_{1g} \rightarrow T_{1g}$ $({}^3T_{2g}) + \nu_6)$, along with three negative $\mathcal{A}$ terms (magnetic dipole line and two t_{1u} sidebands). It is likely that this transition would appear in the 28 000–29 000-cm^{-1} region where very little structure is observed, the progression due to A_{1g} $({}^3T_{1g}) \rightarrow T_{1g}{}^{(1)}$ $({}^3T_{1g})$ having died out. The magnetic moment of the T_{1g} $({}^3T_{2g})$ state is the smallest of the states so far observed, and its magnetic dipole transition moment is extremely small (Table II). Accordingly, lines 24 and 26 (positive $\mathcal{A}$ terms?) are *tentatively* assigned as A_{1g} $({}^3T_{1g}) \rightarrow T_{1g}$ $({}^3T_{2g}) + \nu_6$ and A_{1g} $({}^3T_{1g})$ $\rightarrow T_{1g}$ $({}^3T_{2g}) + \nu_6 + \nu_1$, respectively.

Thus all of the lines in the region 25 500–29 000 cm^{-1} have been assigned except lines 9, 15, and 20, which show extremely weak positive $\mathcal{A}$ terms and very weak absorptions. These lines cannot be convincingly linked with any of the transitions observed in the region, and no other states are predicted here by ligand field calculations. Therefore, it seems not unreasonable to attribute these to impurities.

2. 29 000–34 000-cm^{-1} Region of OsF_6^{2-} (Figure 2). The second intense progression in the spectrum of OsF_6^{2-} lies in the region 29 000–34 000 cm^{-1} and consists of several a_{1g} repeats of lines 1 and 2 (Figure 2). These two lines are separated by about 305 cm^{-1} and each shows a positive $\mathcal{A}$ term, the first more intense. The spacing suggests the interval between a magnetic dipole origin and its $\nu_4(t_{1u})$ sideband. The two features repeat with the same relative intensity throughout the progression, suggesting that they can be attributed to the same electronic transition. Thus we seek an excited state predicted to lie in this general region which can, through the sign of its magnetic moment, account for the MCD. The only state which fits is T_{1g} $({}^3A_{1g})$ which has a large positive magnetic moment (Table II). The only other T_{1g} state in this region $(T_{1g}$ $({}^3E_g{}^{(2)})$ has a magnetic moment of the wrong sign (negative) to be able to produce two positive $\mathcal{A}$ terms (see Table III). There are several T_{2g} states of appropriate energy, but all have magnetic moments of the wrong sign, except T_{2g} $({}^3E_g{}^{(2)})$ (Table II). This state has a negative magnetic moment and could account for the appearance of two positive $\mathcal{A}$ terms assigned as $A_{1g} \rightarrow T_{2g}$ $({}^3E_g{}^{(2)}) + \nu_4(t_{1u})$ and $A_{1g} \rightarrow T_{2g}$ $({}^3E_g{}^{(2)})$ $+ \nu_3(t_{1u})$. However, all calculations predict this state to lie somewhat to higher energy of the most intense line of the observed progression; also, the ν_4–ν_3 spacing (~305 cm^{-1}) in this proposed assignment would be slightly higher than observed previously (~275 cm^{-1}). Furthermore, although no line corresponding to $\nu_6(t_{2u})$ is evident, a shoulder in absorption (3a) and a corresponding feature in the MCD may be discerned which become much clearer in the first a_{1g} repeat (line 7) where a positive $\mathcal{A}$ term is seen. This line may very reasonably be assigned to $\nu_3(t_{1u})$ thus strongly reinforcing the assignment of line 1 as the magnetic dipole origin, $A_{1g} \rightarrow T_{1g}$ $({}^3A_{1g})$. Assignments on this basis are summarized in Table VI. The energy of the first repeat of line 1 (line 3) is taken as the vertical excitation energy of the transition since it is most intense. Again, the a_{1g} progression $(n\nu_1(a_{1g}) + 1\nu(\gamma_u)$, $\gamma_u = t_{1u}, t_{2u})$ is fairly long, n = 0, 1, 2, and 3 being definitely observed. The $\nu_1(a_{1g})$ spacing between line 1 and its first repeat, line 3, is ~660 cm^{-1}, decreasing to ~620 cm^{-1} between the first and second repeats.

Table VI. Assignment of 29 000–34 000 cm^{-1} Region of OsF_6^{2-} (Figure 2)[a]

line no.	sign of $\mathcal{A}$ term	obsd energy, cm^{-1}	calcd energy, cm^{-1} (from Table II)	excited state ($t_{2g}^3e_g$)
1	+	29 265		$T_{1g}(^3A_{1g})$
2	+	29 570		line 1 + $\nu_4(t_{1u})$
3a	*b*	29 820		line 1 + $\nu_3(t_{1u})$
3	+	29 925	29 864	line 1 + $\nu_1(a_{1g})$
4	+	30 075	29 909	$T_{2g}(^3A_{2g}) + \nu_6(t_{2u})$
5	+	30 225		line 1 + $\nu_4 + \nu_1$
6	+	30 380		$T_{1g}(^3E_g^{(2)}) + \nu_6$
7	+	30 470		line 1 + $\nu_3 + \nu_1$
8	+	30 545		line 1 + $2\nu_1$
9	+	30 650	31 831	$T_{2g}(^3E_g^{(2)}) + \nu_4$
10	+	30 740		line 4 + ν_1
11	+	30 860		line 1 + $\nu_4 + 2\nu_1$
12	+	30 950		$T_{2g}(^3E_g^{(2)}) + \nu_3$
13	+	31 060	32 275	line 6 + ν_1
14	+	31 160		line 1 + $3\nu_1$
15	+	31 235		?
16	+	31 285		line 9 + ν_1
17	+	31 365		line 4 + $2\nu_1$
18	+	31 465		line 1 + $\nu_4 + 3\nu_1$
19	+	31 540		?
20	+(?)	31 675		line 6 + $2\nu_1$
21	*b*	31 860		lines 14 and 15 + ν_1
22	*b*	32 175		lines 18 and 19 + ν_1
23	*b*	32 480		lines 14 and 15 + $2\nu_1$
24	*b*	32 760		lines 18 and 19 + $2\nu_1$
25	*b*	33 030		lines 14 and 15 + $3\nu_1$

[a] Refer to footnotes *a* and *b*, Table V. [b] Seen only in absorption.

Unfortunately, it is not really possible to extract quantitative values for Faraday parameters due to large line widths and severe line overlap. Calculated parameters, $\mathcal{A}_1/\mathcal{D}_0$ and $\mathcal{B}_0/\mathcal{D}_0$, for line 1 (Table IV) agree with experiment in order of magnitude, but a quantitative assessment is not possible.

The remaining lines of this region (starting with line 4) cannot be attributed to the transition $A_{1g} \rightarrow T_{1g}$ ($^3A_{1g}$) and have been assigned, as previously, in accord with the calculated order of states. (These lines appear to the high energy side of T_{1g} ($^3A_{1g}$), and so we apparently do not see transitions to the excited states T_{2g} ($^3T_{1g}$) and T_{2g} ($^3T_{2g}$). These two states are predicted to be lower in energy than T_{1g} ($^3A_{1g}$) and to have small magnetic moments (Table II).) In order of increasing energy, the predicted states are T_{2g} ($^3A_{2g}$), T_{2g} ($^3E_g^{(2)}$), and T_{1g} ($^3E_g^{(2)}$). Therefore, line 4 has been assigned to A_{1g} ($^3T_{1g}$) $\rightarrow T_{2g}$ ($^3A_{2g}$) + $\nu_6(t_{2u})$. Line 6 has been assigned to A_{1g} ($^3T_{1g}$) $\rightarrow T_{1g}$ ($^3E_g^{(2)}$) + ν_6, as its first a_{1g} repeat, line 13, is more intense and lies to higher energy than line 9 which can thus be assigned to A_{1g} ($^3T_{1g}$) $\rightarrow T_{2g}$ ($^3E_g^{(2)}$) + ν_4. These and related assignments are summarized in Table VI. It should be emphasized that these assignments, though reasonable, are *not* definitive. The states do have both the predicted energy ordering and magnetic moments with the proper signs. However, line overlap (due to large line widths and to the presence of many states in this region) is severe, and many of the vibrational sidebands (and, in the case of T_{1g} ($^3E_g^{(2)}$), the magnetic dipole origin) are not observed. We are also unable to account for lines 15 and 19, which remain unassigned.

3. Splitting of the No-Phonon Magnetic Dipole Origin of OsF_6^{2-} (Line 1, Figure 1). Figure 3 shows the observed splitting of the first spectral line, assigned as the no-phonon magnetic dipole origin of the transition A_{1g} ($^3T_{1g}$) $\rightarrow T_{1g}^{(1)}$ ($^3T_{1g}$). This line is the sharpest in the spectrum, having a zero-field half-width (at (1/e) × (peak height)) ≈ 4.8 cm^{-1}. Careful examination indicates that the absorption line has

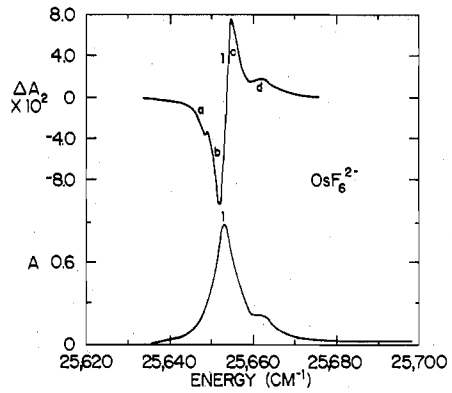

Figure 3. Absorption (A) and MCD (ΔA) spectrum of the magnetic dipole origin, $A_{1g} \rightarrow T_{1g}^{(1)}$ ($^3T_{1g}$), in Cs_2GeF_6:Os^{4+}, at 1 T and ~4.2 K. Notation and conversion factors are as in Figure 1.

three components, the obvious shoulder (Figure 3) at higher energy, the main line, and a barely perceptible shoulder to low energy. The MCD of the main line shows a very clear $\mathcal{A}$ term (Figure 3) proving that it contains (at least) two subcomponents. Thus four components, labeled a–d in Figure 3, must be accounted for. Clearly, only three components are possible for the transition $A_{1g} \rightarrow T_{1g}$. Higher field data (maximum 5 T) shows that the lines do not scale linearly with field, particularly lines b and c, which are more intense per unit field at the lower field. Lines c and d show a greater energy spacing (~8.6 cm^{-1} at 1 T) than do lines a and b (~3.4 cm^{-1} at 1 T). The energy spacing of lines c and d is found to decrease somewhat at higher fields.

We postulate that the zero-field splitting is due to a reduction in the octahedral symmetry at the Os^{4+} substitutional site. In view of the nonlinearity of the MCD, the usual perturbation approach ($\mathcal{A}$, $\mathcal{B}$, $\mathcal{C}$ language[16]) is not applicable, and one must return to the general formula for $\epsilon_\pm$.[25] Input data for a theoretical calculation include the observed transition energy, the calculated $T_{1g}^{(1)}$ ($^3T_{1g}$) g value (Table II), the assumption of a line-shape function (Gaussian) shifting rigidly with field, and the fact (determined by X-ray photographs) that the field (and light propagation) was along a (112) crystallographic axis. Specifying field and temperature, and assuming a distortion model, one may diagonalize the T_{1g} state with respect to the Zeeman and distortion perturbations to evaluate $\epsilon_\pm$ (and therefore $A = Cl(\epsilon_+ + \epsilon_-)$ and $\Delta A = Cl(\epsilon_- - \epsilon_+)$. ($Cl$ = concentration × path length.)

It is found that the experimental absorption and MCD patterns *for components b, c, and d* can be reproduced reasonably well as a function of field if it is assumed that the Os^{4+} site is tetragonally distorted with equal probability along the x, y, and z molecular axes (F–Os bond directions). The best fit is obtained with distortion parameter (Table VII), d = 3.25 ± 0.25 cm^{-1}. A similar attempt to explain the data assuming a trigonal distortion was unsuccessful.

Assuming the essential correctness of this analysis, it is clear that line a must arise from a different transition, but no other electronic state is predicted to lie within ~1000 cm^{-1} of $A_{1g} \rightarrow T_{1g}^{(1)}$. It is possible that line a reflects a small concentration of OsF_6^{2-} at a slightly different site in the host in which case its corresponding positive $\mathcal{A}$ term lobe would be extremely hard to see superimposed on the large $\mathcal{A}$ term (lines b and c). Alternatively, a might be a "hot" line arising from a very low energy (~3 cm^{-1}) lattice mode. No other line in the spectrum is sufficiently sharp to see splittings as small as those observed for line 1.

B. IrF_6^{2-}. The aqueous solution spectrum[26] and diffuse reflectance studies[9,15,27] of IrF_6^{2-} have been reported, but no low-temperature crystal work appears to have been done. We here report low-temperature MCD and absorption spectra of

Table VII. Tetragonal Distortion Matrices for the First-Order Splitting of a T_1 state

$H^z{}_{tet}$[a]	x	y	z	$H^z{}_{tet}$[b]	+1	0	−1	$H^{x,y}{}_{tet}$[c]	+1	0	−1
x	−d			+1	−d			+1	d/2		∓3d/2
y		−d		0		2d		0		−d	
z			2d	−1			−d	−1	∓3d/2		d/2

[a] For a tetragonal distortion along the molecule-fixed z axis. x, y, and z are abbreviations respectively for T_1x, T_1y, T_1z.[18] For a tetragonal distortion along y or x, interchange 2d and (−d) appropriately. [b] For a tetragonal distortion along the molecule-fixed z axis in the complex basis where +1, 0, −1, respectively, designate $T_1 + 1$, $T_1 0$, $T_1 - 1$ with $T_1 \pm 1 = \mp i/2^{1/2}(T_1x \pm iT_1y)$, $T_1 0 = iT_1z$.[18] [c] For a tetragonal distortion along the molecule-fixed x (upper signs) or y (lower signs) axis in the complex basis.[18]

Table VIII. Assignment of the $E''_g(^2T_{2g}) \rightarrow U'_g(^2T_{2g})$ Intraconfigurational Transitions of IrF_6^{2-} (Figure 4)

line no.	sign of $\mathcal{C}$ term	obsd energy, cm^{-1} (based on absorption spectrum)	assignment
1	+	6370	$U'_g(^2T_{2g}{}^{(1)})$(magnetic dipole)
1a		6435	line 1 + lattice mode
1b		6515	?
2	+	6590	line 1 + $\nu_6(t_{2u})$
3	+	6640 (6697)[a]	line 1 + $\nu_4(t_{1u})$
3a		6695	?
3b		6780	?
3c		6875	?
4	+	6930	line 1 + $\nu_3(t_{1u})$
4a		7005	?
4b		7090	?
5	+	7125	line 1 + $\nu_1(a_{1g})$
5a		7205	line 1a + ν_1
6	+	7355	line 1 + ν_6 + ν_1
7	+	7395	line 1 + ν_4 + ν_1
7a		7435	line 3a + ν_1
7b		7540	line 3b + ν_1
7c		7585	?
7d		7630	line 3c + ν_1
8	+	7695	line 1 + ν_3 + ν_1
8a		7740	line 4a + ν_1
9	+	7870	line 1 + $2\nu_1$
9a		7895	line 1a + $2\nu_1$ (?)
9b		8195	line 1 + ν_4 + $2\nu_1$ (?)

[a] Calculated value based on ligand field parameters (in cm^{-1}) $B = 641$, $C = 3140$, $Dq = 2450$, and $\zeta = 3500$.

Table IX. Excited-State Vibrational Frequencies (cm^{-1}) Observed for IrF_6^{2-}

$\nu_1(a_{1g})$	$\nu_3(t_{1u})$[a]	$\nu_4(t_{1u})$	$\nu_6(t_{2u})$
755[b] ~500–550[c]	560[b]	270[b]	220[b]

[a] A ground-state value of $\nu_3 = 568$ cm^{-1} has been reported by Peacock and Sharp.[28] [b] $U'_g(^2T_{2g}(t_{2g}{}^5))$ state (Figure 4). [c] $(t_{2g}{}^4e_g)$ configuration (Figure 6).

Table X. Faraday Parameters for Magnetic Dipole Transitions of IrF_6^{2-} [a]

A	J	$\mathcal{A}_1/\mathcal{D}_0$	$\mathcal{C}_0/\mathcal{D}_0$
E''_g	E''_g	$2(G + F)$	$2F$
E''_g	U'_g	$-1/_2H - 3/_2I - F$	$-F$

[a] A refers to the ground and J to the excited state: $E = \langle E'\alpha'|L_z + 2S_z|E'\alpha'\rangle$, $F = \langle E''_A\alpha''|L_z + 2S_z|E''_A\alpha''\rangle$, $G = \langle E''_J\alpha''|L_z + 2S_z|E''_J\alpha''\rangle$, $H = \langle U'\kappa|L_z + 2S_z|U'\kappa\rangle$, and $I = \langle U'\lambda|L_z + 2S_z|U'\lambda\rangle$.

Table XI. Calculated $\mathcal{C}_0/\mathcal{D}_0$ for Vibronic Transitions from $E''_g(^2T_{2g}{}^{(1)}(t_{2g}{}^5))$ of IrF_6^{2-} [a]

symmetry of mixing state	symmetry of vibration	$\mathcal{C}_0/\mathcal{D}_0$
E''_u	t_{1u}	−0.376[b,c]
E'_u	t_{2u}	−0.376[b,c]
E''_u	t_{1u} or t_{2u}	−2.26[c,d]
U'_u	t_{1u} or t_{2u}	[b,e]
U'_u	t_{1u} or t_{2u}	1.12[c,d]

[a] Based on the magnetic moments of Table XII and using the irreducible tensor method.[18-21] [b] For transition to $U'_g(T_{2g}{}^{(1)}(t_{2g}{}^5))$ assuming ground-state mixing only. [c] Ignoring cross terms between different symmetry mixing states. Inclusion of such terms precludes the cancellation of transition dipole matrix elements.[20,21] [d] For transition to E'_g, E''_g, or U'_g. [e] More detail about the mixing state is required.

Ir^{4+} ($5d^5$) doped into the cubic host Cs_2GeF_6. The results permit some characterization of the interconfigurational d–d transitions in addition to analysis of the intraconfigurational transition within the spin–orbit split $^2T_{2g}$ ground term.

1. The Intraconfigurational $[E''_g\ (^2T_{2g}) \rightarrow U'_g\ (^2T_{2g})]$ Spectrum of IrF_6^{2-}. The intraconfigurational transition, $E''_g\ (^2T_{2g}\ (t_{2g}{}^5)) \rightarrow U'_g\ (^2T_{2g}\ (t_{2g}{}^5))$, of $IrCl_6^{2-}$ has been examined at low temperature in both MCD and absorption by Keiderling et al.[22] The low-temperature MCD and absorption spectra for this transition in IrF_6^{2-} are shown in Figure 4. The resolution of the MCD, as has been previously mentioned, is poor, only broad positive $\mathcal{C}$ terms (positive MCD) being observed. The absorption spectrum, however, is much better resolved and shows vibronic detail very similar to that observed by Keiderling et al.[22] for $IrCl_6^{2-}$. The principal features observed for IrF_6^{2-} are assigned, as in $IrCl_6^{2-}$, as a no-phonon magnetic dipole origin (line 1) followed by three electric dipole vibrational sidebands arising from the coupling of the parity-forbidden transition to ungerade vibrational modes of IrF_6^{2-} ($\nu_6(t_{2u})$, $\nu_4(t_{1u})$, and $\nu_3(t_u)$; lines 2, 3, and 4). Table VIII shows these assignments which are straightforward except for some very weak features which probably reflect deviations from the $k = 0$ approximation. The A_{1g} progression is very short, repeating essentially only once as in $IrCl_6^{2-}$. This is as expected for an intraconfigurational transition since no excitation of an electron to the more antibonding e_g orbital is involved. The two potential surfaces should be very similar.

The a_{1g} progression ($n\nu_1(a_{1g}) + 1\nu(\gamma_u)$, $\gamma_u = t_{1u}, t_{2u}$) of the $E''_g \rightarrow U'_g$ band of IrF_6^{2-} shows greatest intensity for $n = 0$, and the energy of line 3 (6640 cm^{-1}) is taken as the equilibrium vertical excitation energy. This differes considerably from the value in $IrCl_6^{2-}$ (approximately 5284 cm^{-1}).[22] IrF_6^{2-} is predicted to be less covalent, and thus its effective spin–orbit coupling parameter (ζ) is expected to be larger, resulting in a larger splitting of the $^2T_{2g}$ ground term. In fitting the U'_g ($^2T_{2g}$) and higher excited states (to be discussed next), a value of $\zeta = 3500$ cm^{-1} was found best. For $IrCl_6^{2-}$ a value of 2800 cm^{-1} ($\pm\approx 200$ cm^{-1}) was required (but based only on the U'_g ($^2T_{2g}$) excited state), unless unlikely Dq, B, and C values were used.[22] Other obvious differences from $IrCl_6^{2-}$ are the fact that the magnetic dipole origin is more intense relative to the vibronic lines and that the $\nu_4(t_{1u})$ vibronic line is somewhat more intense than $\nu_6(t_{2u})$ whereas the latter dominates in $IrCl_6^{2-}$.

Table IX shows the U'_g excited state vibrational frequencies observed for IrF_6^{2-}.

Turning now to the MCD of the intraconfigurational band (Figure 4), we observe only $\mathcal{C}$ terms because the large slit widths (necessarily) used integrate to zero the $\mathcal{A}$ terms which are undoubtedly present. The magnetic dipole origin (line 1) shows a positive $\mathcal{C}$ term in agreement with theory (Tables X and XII).

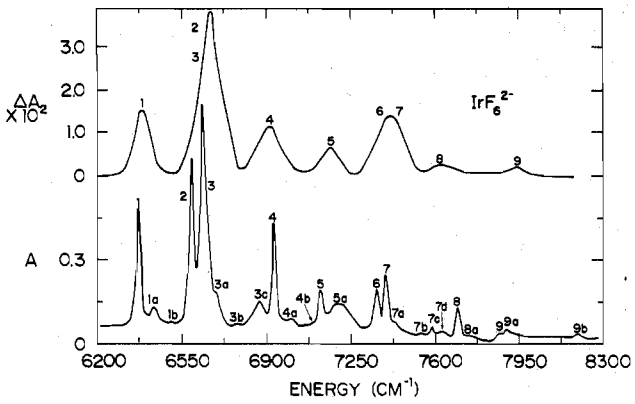

Figure 4. Absorption spectrum (A = absorbance) and MCD [$\Delta A = (A_L - A_R)$ per tesla] for the intraconfigurational transition, E''_g ($^2T_{2g}$) → U'_g ($^2T_{2g}$), of Cs_2GeF_6:Ir^{4+}. The MCD spectrum, recorded at 1.5 K, is not fully resolved (spectral slit width ~100 cm^{-1}) and is strongly saturated. The absorption spectrum, recorded at 4.2 K, is fully resolved. Multiplication by 35 converts A to ϵ (molar extinction coefficient).

Table XII. Calculated Magnetic Moments and Energies of Selected States of IrF_6^{2-} [a]

state[b]	component	magnetic moment[c]	calcd energy, cm^{-1}
$E''_g(^2T_{2g}^{(1)}(t_{2g}^5))$	α''	−1.129	0.00
$U'_g(^2T_{2g}^{(1)}(t_{2g}^5))$	κ	0.068	6 697
	λ	0.194	
$U'_g(^2T_{1g}^{(1)}(t_{2g}^4e_g))$	κ	0.618	25 237
	λ	0.707	
$E''_g{}^{(1)}(^2T_{2g}(t_{2g}^4e_g))$	α''	0.932	26 944
$E'_g(^2T_{1g}^{(1)}(t_{2g}^4e_g))$	α'	0.145	28 560
$E''_g{}^{(2)}(^2T_{2g}(t_{2g}^4e_g))$	α''	−0.496	29 437
$U'_g(^2T_{2g}^{(2)}(t_{2g}^4e_g))$	κ	0.670	30 554
	λ	−0.759	
$U'_g(^2E_g(t_{2g}^4e_g))$	κ	−1.616	31 679
	λ	1.155	
$U'_g(^2T_{1g}^{(2)}(t_{2g}^4e_g))$	κ	−0.289	33 250
	λ	−0.557	

[a] Using the ligand field parameters (in cm^{-1}), $B = 641$, $C = 3140$, $Dq = 2450$, $\zeta = 3500$, and the notation of ref 18. [b] Superscripts (1) and (2) differentiate between states of the same symmetry coming from the same term and also between terms having the same term symbol. The term in parentheses designates the single most important contributor to the state. [c] In Bohr magnetons for the operator, $(L_z + 2S_z)$.

Detailed analysis of the MCD sidebands is precluded by the complexity of the vibronic coupling mechanism. In particular, mixing states of more than one symmetry can contribute to the intensity. Various cases are summarized in Table XI. (This complexity is in sharp contrast to the OsF_6^{2-} case where only T_{1u} mixing states are possible and where the A_{1g} ground state allows the simultaneous inclusion of both ground- and excited-state mixing.[11]) Positive $\mathcal{C}_0$ terms are observed (Figure 4) indicating (Table XI) that U'_u mixing states are contributing significantly to the intensity, as was observed previously for $IrCl_6^{2-}$.[22]

2. Interconfigurational Transitions ($t_{2g}^5 \rightarrow t_{2g}^4e_g$) (Figures 5–7). The spectrum of IrF_6^{2-} in the 19 000–41 000-cm^{-1} region consists of many overlapping lines whose MCD shows both $\mathcal{A}$ and $\mathcal{C}$ terms. The latter are manifested by the roughly $1/T$ dependence of the MCD throughout and the former may be seen as superimposed progressions.

To analyze the spectrum, we first use the signs of the broad $\mathcal{C}$ terms to determine the symmetry of the dominant mixing state. (Since most of the intensity is in vibronic sidebands, we assume that the sign of the composite $\mathcal{C}$ terms (which include both origin and sidebands) will be determined by the vibronic mechanism.) Table XI shows that the sign of a vibronic $\mathcal{C}$ term is determined by the symmetry of the mixing state involved, E''_u and U'_u giving negative and positive values, respectively (assuming excited state mixing only). Signs of $\mathcal{A}$ terms and energy considerations are then used to locate particular excited states.

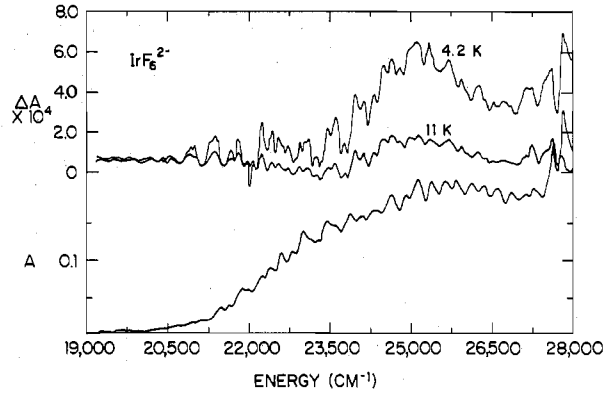

Figure 5. Absorption spectrum (A) at ~9 K and MCD spectrum (ΔA) at 4.2 and 11 K for the low-energy interconfigurational region of Cs_2GeF_6:Ir^{4+}. Notation and conversion factors are as in Figure 4.

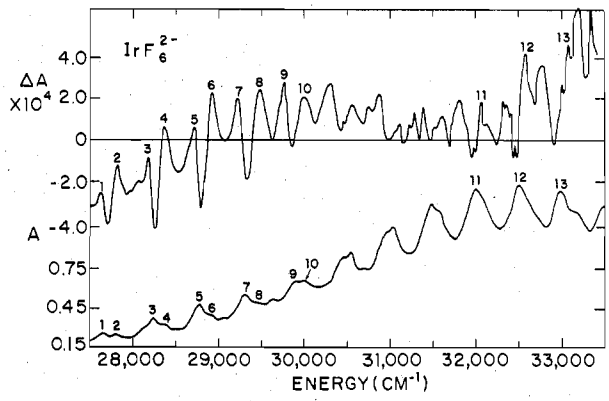

Figure 6. Absorption spectrum (A) at ~9 K and MCD spectrum (ΔA) at 36 K for the middle-energy interconfigurational region of Cs_2GeF_6:Ir^{4+}. The high temperature of the MCD greatly reduces the amplitude of the $\mathcal{C}$ terms and makes the $\mathcal{A}$ terms much more distinct though the baseline is somewhat unreliable. Low-temperature measurements show that the MCD in this figure in the 27 500–31 000-cm^{-1} region is superimposed on a broad, positive $\mathcal{C}$ term background and that in the 31 000–33 500-cm^{-1} region is superimposed on a broad, negative $\mathcal{C}$ term background. Notation and conversion factors are as in Figure 4.

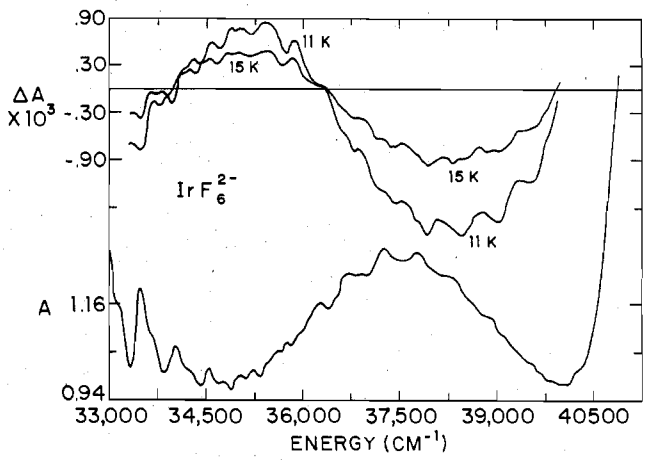

Figure 7. Absorption spectrum (A) at ~9 K and MCD spectrum (ΔA) at 11 and 15 K for the high-energy interconfigurational region of Cs_2GeF_6:Ir^{4+}. Notation and conversion factors are as in Figure 4.

Table XIII. Calculated $\mathcal{A}_1/\mathcal{D}_0$ for Interconfigurational Transitions in IrF_6^{2-} [a]

excited state ($t_{2g}^4e_g$)	magnetic dipole $\mathcal{A}_1/\mathcal{D}_0$	vibronic $\mathcal{A}_1/\mathcal{D}_0$ (E''_u mixing)		vibronic $\mathcal{A}_1/\mathcal{D}_0$ (U'_u mixing)	
		t_{1u}	t_{2u}	t_{1u}	t_{2u}
$U'_g(^2T_{1g}^{(1)})$	−0.24	−3.18	−1.40	–[b]	–[b]
$E''_g{}^{(1)}(^2T_{2g})$	−0.40	−2.88	–[c]	+1.68	+0.20
$E'_g(^2T_{1g}^{(1)})$	–[c]	–[c]	−2.36	+0.98	+1.22
$E''_g{}^{(2)}(^2T_{2g})$	−3.26	−1.92	–[c]	+0.84	+1.62
$U'_g(^2T_{2g}^{(2)})$	+1.94	−1.72	−1.84	–[b]	–[b]
$U'_g(^2E_g)$	+0.20	−2.88	−3.48	–[b]	–[b]
$U'_g(^2T_{1g}^{(2)})$	+2.10	−1.60	−2.74	–[b]	–[b]

[a] Based on Table XII magnetic moments. General formulas (but using the definitions of ref 8) may be found in the Ph.D. dissertation of L. C. Weiss, University of Virginia, Aug 1977. [b] More detailed information about mixing state is required. [c] Forbidden by symmetry.

The 27 500–35 500-cm^{-1} region shows the best resolved MCD features. At the low-energy end we observe a progression of "double $\mathcal{A}$ term" line shapes, labeled 1, 2; 3, 4; ... (Figure 6). That is, the MCD[16] consists of two overlapping $\mathcal{A}$ terms of opposite sign, approximately 110 cm^{-1} apart, with the negative term[16] at lower energy. Two corresponding features are observed in absorption. The 110-cm^{-1} spacing corresponds to no reasonable vibrational interval (see Table IX), and careful examination of the progression (both in absorption and MCD) shows that the relative intensities of the two features change significantly, the lower energy line "growing in" as one moves through the progression. It thus seems clear that these two features correspond to different electronic transitions. The higher energy feature reaches maximum intensity at $n = 2$ in the progression (line 6) and the other, most probably, at $n = 3$ (line 7); the energies of these two lines are thus taken as the equilibrium vertical excitation energies of the transitions (see Table XIV), and thus the positive $\mathcal{A}$ term is associated with the *lower* energy transition and vice versa. The first repeat in the progression corresponds to an a_{1g} frequency of 550 cm^{-1}.

"Complete" ligand field calculations have been carried out for many different parameter sets, and only two states in this general energy region fall within 1000 cm^{-1} of each other. These are $E'_g(^2T_{1g}^{(1)})$ and $E''_g{}^{(2)}(^2T_{2g})$ (E''_g being higher). Broad positive $\mathcal{C}$ terms dominate the overall MCD in the 27 500–30 500-cm^{-1} region (though this is not obvious in Figure 6 because of the relatively high temperature used to highlight the $\mathcal{A}$ terms). This indicates a dominant mixing state of U'_u symmetry (see Table XI) for vibronic lines in the region. Calculated values of $\mathcal{A}_1/\mathcal{D}_0$ for vibronic transitions to the E'_g $(^2T_{2g}^{(1)})$ and $E''_g{}^{(2)}$ $(^2T_{2g})$ excited states via U'_u symmetry mixing are summarized in Table XIII. It can be seen for both t_{1u} and t_{2u} vibrations that calculated $\mathcal{A}_1$ values are positive for transitions to either of the two excited states under discussion. However, in the case of the E''_g symmetry excited state, a magnetic dipole transition is allowed, and such a transition has a negative $\mathcal{A}_1$. The signs of the calculated $\mathcal{A}$ parameters thus support the assignment suggested by energy considerations if one attributes the observed positive $\mathcal{A}$ term to a vibronic transition (via U'_u mixing) to the E'_g $(^2T_{1g}^{(1)})$ excited state and the observed negative $\mathcal{A}$ term to a magnetic dipole transition to the $E''_g{}^{(2)}$ $(^2T_{2g})$ excited state. The feature assigned to the magnetic dipole line is the sharper of the two, as might be expected. Assignments of the specific lines are given in Table XIV. The a_{1g} progressions peak at $n = 2$ or 3, indicating a significant difference between the ground- and excited-state potential surfaces in both cases.

Turning to the remainder of the 27 500–33 500-cm^{-1} region, it is found that the only other clearly distinguishable MCD lies to higher energy and consists of a progression of three large positive $\mathcal{A}$ terms (lines 11, 12, and 13, Figure 6). These are approximately 500 cm^{-1} apart, again presumed to be a $\nu_1(a_{1g})$ spacing, and the progression is somewhat shorter than the transition discussed just previously Thus, values of 500–550 cm^{-1} for $\nu_1(a_{1g})$ have been observed for the excited states of the interconfigurational transitions of IrF_6^{2-}, whereas a value of approximately 755 cm^{-1} was observed for the U'_g excited state of the E''_g $(^2T_{2g}) \rightarrow U'_g$ $(^2T_{2g})$ intraconfigurational transition. This is a rather large difference which can presumably be rationalized at least in part by the more antibonding nature of the excited configuration (for example, $t_{2g}^4e_g$ vs. t_{2g}^5). Furthermore, it was noted[22] in $IrCl_6^{2-}$ that ν_1 in the U'_g $(^2T_{2g}$ $(t_{2g}^5))$ state was "abnormally" high—about 12% higher than the ground-state value. (Unfortunately, a ground-state value for ν_1 in IrF_6^{2-} does not seem to have been reported.)

Table XIV. Assignment of the Interconfigurational Transitions of IrF_6^{2-}

line no.	obsd sign of $\mathcal{A}$ term	obsd energy,[a] cm^{-1}	calcd energy,[b] cm^{-1}	excited state ($t_{2g}^4e_g$)[c]
1	−	~27 670		$E''_g{}^{(2)}(^2T_{2g})$(magnetic dipole)
2	+	~27 780		$E'_g(^2T_{1g}^{(1)}) + \nu_i$
3	−	~28 220		line 1 + ν_1
4	+	~28 330		line 2 + ν_1
5	−	~28 760		line 1 + $2\nu_1$
6	+	~28 870	28 560	line 2 + $2\nu_1$
7	−	~29 290	29 437	line 1 + $3\nu_1$
8	+	~29 400		line 2 + $3\nu_1$ + (?)
9	−	~29 850		line 1 + $4\nu_1$ + (?)
10	+	~29 910		line 2 + $4\nu_1$ + (? + ν_1)
11	+	~32 000		$U'_g(^2T_{1g}^{(2)})$(magnetic dipole)
12	+	~32 500		line 11 + ν_1
13	+	~33 000	33 250	line 11 + $2\nu_1$

[a] Based on MCD of Figure 6. [b] For the ligand field parameters (in cm^{-1}), $B = 641$, $C = 3140$, $Dq = 2450$, $\zeta = 3500$. [c] ν_i represents the unresolved composite of ν_6, ν_4, ν_3.

In assigning this progression (lines 11–13), account was taken of the fact that all crystal field calculations show three states falling in this general energy region, namely, U'_g $(^2T_{2g}^{(2)})$, U'_g (^2E_g), and U'_g $(^2T_{1g}^{(2)})$. The broad $\mathcal{C}$ term of the region is negative indicating an E''_u mixing state for vibronic lines (Table XI). Values were calculated for both vibronic (via E''_u mixing) and magnetic dipole transitions to the three U'_g states (Table XIII). For each, only a magnetic dipole transition gives a positive $\mathcal{A}_1$. Calculated magnetic dipole transition moments for the three excited states are all the same order of magnitude (~0.1) and are thus not helpful in making the assignment. It was found, however, that only the U'_g $(^2T_{1g}^{(2)})$ choice would permit a fit of the energies of the previously assigned E'_g $(^2T_{1g}^{(1)})$ and $E''_g{}^{(2)}$ $(^2T_{2g})$ states. Attempts to assign the observed progression to the U'_g $(^2T_{2g}^{(2)})$ or the U'_g (^2E_g) excited state resulted in either the energies of the E'_g, E''_g pair being too high or the U'_g state being too low. Assignments are summarized in Table XIV. Maximum MCD intensity is observed for line 13 whose energy has been taken as the equilibrium vertical excitation. The U'_g $(^2T_{2g}^{(2)})$ and U'_g (^2E_g) excited states probably lie somewhere between the observed E'_g $(^2T_{1g}^{(1)})$, $E''_g{}^{(2)}$ $(^2T_{2g})$ pair and the observed U'_g $(^2T_{1g}^{(2)})$ excited state, but the MCD in this region is very nondescript, and a more precise estimate of the energies of these two states is not possible.

The MCD of the lower-lying (19 000–27 500 cm^{-1}) region (Figure 5) consists of broad positive $\mathcal{C}$ terms (centered at approximately 25 000 cm^{-1}), indicative of U'_u symmetry mixing. Many overlapping progressions of $\mathcal{A}$ terms appear to be built on the broad $\mathcal{C}$ term feature, and we were not able

to resolve these sufficiently to suggest detailed assignments. However, the previous analysis leads one to believe that the two lowest-lying "spin-allowed" states, U'_g ($^2T_{1g}^{(1)}$) and $E''_g{}^{(1)}$ ($^2T_{2g}$), probably lie in this region. The energies of these two excited states according to final crystal field calculations are shown in Table XII to be ~25 250 and ~27 000 cm^{-1}, respectively. Six "spin-forbidden" states are predicted to lie in the 20 000–23 000-cm^{-1} region. (Here, states termed "spin-forbidden" have strong-field wave functions showing 83–94% spin-forbidden character; the two "spin-allowed" states have 84% (U'_g) and 89% (E''_g) spin-allowed character.)

The rest of the data lies in the 33 500–41 000-cm^{-1} region and is shown in Figure 7. The MCD consists of two broad, oppositely signed $\mathscr{C}$ term regions centered at about 35 250 cm^{-1} (positive) and about 38 250 cm^{-1} (negative), indicating U'_u and E''_u mixing, respectively. The structure is poorly resolved, and specific interpretation of the features is not possible. Final crystal field calculations predict nine excited states in this region. Beyond 41 000 cm^{-1}, the spectrum becomes much more intense, probably due to the onset of ligand-to-metal charge-transfer transitions. An intense band at 47 800 cm^{-1} in the diffuse reflectance spectrum has been assigned as such.[9,10]

Conclusions

Once again the great utility of MCD in interpreting complex electronic spectra is evident. While specific assignments for many detailed features are lacking and ambiguities remain, we believe we have assigned enough features convincingly to permit a significant refinement of previous ligand field parameters for octahedral Os^{4+} and Ir^{4+} species. We do not think this would have been possible without the MCD analysis.

For Cs_2GeF_6:Os^{4+}, the ligand field parameters B = 625 cm^{-1}, C = 2969 cm^{-1}, Dq = 2450 cm^{-1}, and ζ = 2800 cm^{-1} have been chosen, first, to fit the four most definitive assignments ($T_{1g}^{(1)}$ ($^3T_{1g}$), $T_{1g}^{(2)}$ ($^3T_{1g}$), T_{2g} ($^3E_g^{(1)}$), and T_{1g} ($^3A_{1g}$)) and, second, to give a reasonable fit of all of the assigned states. Throughout our parameter variations, we have used the same C/B ratio (4.75) employed by Allen et al.[9,15] in their analysis of the diffuse reflectance spectrum of OsF_6^{2-}. However, our resultant B and C values are higher than theirs (B = 500 cm^{-1}, C = 2375 cm^{-1}) and give a considerably higher nephelauxetic ratio, β ($=B_{complex}/B_{free\ ion}$ where $B_{free\ ion}$ = 677 cm^{-1} [9]), specifically, 0.92 vs. 0.74. Our Dq value (2450 cm^{-1}) is somewhat lower than the value (2600 cm^{-1}) reported by Allen et al. Finally, our analysis of the low-temperature crystal data gives a value of 2800 cm^{-1} for ζ which is quite close to the value of Allen et al. (2900 cm^{-1}). It must be remembered that none of the intraconfigurational d–d bands of OsF_6^{2-} were observed at low temperature due to the low concentration of Os^{4+} in the crystals, and as a result, the spin–orbit splitting of the ground state was not included in the ligand field fit. Such bands were, however, observed in the diffuse reflectance spectra, strengthening credence in the ζ value. A study of the intraconfigurational d–d bands of OsF_6^{2-} under low-temperature, high-resolution conditions would clearly be of interest.

Although the low-temperature d–d spectrum of IrF_6^{2-} lacked the vibronic detail displayed by OsF_6^{2-}, it proved possible to assign four excited states, and the ligand field parameter set B = 641 cm^{-1}, C = 3140 cm^{-1}, Dq = 2450 cm^{-1}, and ζ = 3500 cm^{-1} produced the best fit. Again the C/B ratio (4.90) of Allen et al.[9,15] was employed.

Comparison of this Ir^{4+} parameter set with that obtained by Allen et al.[9,15] from the room-temperature diffuse reflectance spectrum of K_2IrF_6 reveals some interesting differences. Their spectrum, as assigned, was best fit by the parameters B = 510 cm^{-1}, C = 2499 cm^{-1}, Dq = 2700 cm^{-1}, and ζ = 3300 cm^{-1}, differing most noticeably from ours in the value of Dq. This difference results from the fact that in our analysis, the observed MCD band at about 25 000 cm^{-1} is assigned to two "spin-allowed" transitions, the "spin-forbidden" states lying to lower energy, whereas Allen et al. assigned bands at 19 800 and 24 900 cm^{-1} to the "spin-forbidden" $^2T_{2g} \rightarrow {}^4T_{1g}$ and $^2T_{2g} \rightarrow {}^4T_{2g}$ transitions. Their assignments were based upon the work of Douglas,[29] who assigned the $IrCl_6^{2-}$ absorption in the 18 670–19 000 and 20 800–22 200 cm^{-1} region to spin-forbidden ligand field transitions to the $^4T_{1g}$ and $^4T_{2g}$ levels, respectively. However, low-temperature MCD and absorption studies of $IrCl_6^{2-}$ by Piepho et al.[4] showed that the observed absorption was due to parity-forbidden charge-transfer transitions. If one assumes with Allen et al. that the positions of the $^4T_{1g}$ and $^4T_{2g}$ levels should not show much change on passing from $IrCl_6^{2-}$ to IrF_6^{2-},[15] the low-temperature data reported here for IrF_6^{2-} and that of Piepho et al. for $IrCl_6^{2-}$ are consistent and contradict the assignments of Douglas and of Allen et al. Thus the value 2450 cm^{-1} for Dq should be clearly preferable to the 2700-cm^{-1} value of Allen et al. Their values of B and C once again give a lower neuphalexetic ratio. Agreement between the two values of ζ is fairly good, with the low-temperature data providing the higher value.

It is also of interest to compare the set of parameters obtained for IrF_6^{2-} with that obtained for OsF_6^{2-}. In passing from OsF_6^{2-} to IrF_6^{2-}, B and C have increased. Such increases are expected, since for a given oxidation state, the size of an ion decreases with increasing number of d electrons, decreasing the mean radial displacement of the d shell and therefore increasing the mutual interelectronic repulsion.[30,31] At the same time, however, it is observed that the nephelauxetic ratio ($B_{complex}/B_{free\ ion}$) has decreased on passing from OsF_6^{2-} to IrF_6^{2-} according to values for $B_{free\ ion}$ given by Allen et al. ($B_{Os^{4+}}$ = 677 cm^{-1}, $B_{Ir^{4+}}$ = 712 cm^{-1}),[9] indicating an increasing tendency toward covalency as is generally observed as one moves from left to right across a transition series.[10] $\zeta_{Ir^{4+}}$ is, as expected, larger than $\zeta_{Os^{4+}}$, whereas the value of Dq is approximately the same for both ions.

It is interesting to estimate the location of the interconfigurational d–d transitions in the corresponding hexahalides, $OsCl_6^{2-}$ and $IrCl_6^{2-}$. We use the estimated ligand field parameters (in cm^{-1}) B = 542, C = 2573, Dq = 2178, and ζ = 2650 ($OsCl_6^{2-}$) and B = 534, C = 2617, Dq = 2178, and ζ = 2800 ($IrCl_6^{2-}$). Then the $A_{1g} \rightarrow T_{1g}^{(1)}$ ($^3T_{1g}$) origin (the first strong feature observed in OsF_6^{2-}) is calculated to occur at ~23 000 cm^{-1} in $OsCl_6^{2-}$, and the $E''_g \rightarrow U'_g$ ($^2T_{1g}^{(1)}$) origin (calculated to occur at ~25 250 cm^{-1} in IrF_6^{2-}) is calculated to occur at ~22 000 cm^{-1} in $IrCl_6^{2-}$. No lines have been reported[5,17b] at ~23 000 cm^{-1} in $OsCl_6^{2-}$, and it is possible that this origin could be observed in a concentrated crystal. Such a d–d spectrum would quickly be swamped by the onset of strong charge-transfer absorption beyond 24 000 cm^{-1}.[5] In $IrCl_6^{2-}$, some weak features observed at ~22 000 cm^{-1} were tentatively assigned to d–d transitions.[4] Again such a d–d spectrum will quickly be swamped by the onset of strong charge-transfer bands beyond ~22 800 cm^{-1}.[4]

A low-temperature luminescence and absorption study has recently been reported on PtF_6^{2-} doped into Cs_2GeF_6, Cs_2SiF_6, and Rb_2SiF_6.[32] Highly resolved ligand field spectra were observed, and electronic assignments have been proposed. It was also suggested[32] on the basis of the PtF_6^{2-} analysis that in 5d transition-metal complexes, the first observed absorption peak for interconfigurational transitions will involve several a_{1g} quanta; i.e., magnetic dipole origins will not be observed. This generalization is unwarranted since such origins are clearly seen in our OsF_6^{2-} spectra and are quite likely seen in IrF_6^{2-}.

Acknowledgment. We are much indebted to Professor W. Preetz for the sample of Cs_2IrF_6, to Dr. Elmars R. Krausz for

making instrumental modifications permitting the infrared MCD measurements on IrF_6^{2-} and for much additional help, to Dr. Hans Güdel for the loan of infrared gratings, to Drs. R. O. Allen and S. Williams for performing the neutron activation analyses, and to Dr. E. Sinn for an X-ray determination of the crystal orientation of $Cs_2GeF_6:Os^{4+}$. Last, but not least, we thank Dr. Warren C. Yeakel for many helpful discussions and for the use of his computer programs to calculate the tetragonal distortion parameter. L.C.W. wishes to acknowledge support of NDEA and Governor's fellowships. This work was supported by a grant from the National Science Foundation.

Registry No. OsF_6^{2-}, 38966-66-4; IrF_6^{2-}, 21265-41-8; Cs_2GeF_6, 16919-21-4; Cs_2IrF_6, 16923-82-3; H_2OsCl_6, 27057-71-2.

References and Notes

(1) Based on a Ph.D. thesis submitted by Lucy Cline Weiss, University of Virginia, Aug 1977.
(2) (a) P. J. Stephens, *Adv. Chem. Phys.*, **35**, 197 (1976); (b) P. J. Stephens, *Annu. Rev. Phys. Chem.*, **25**, 201 (1974), and references therein.
(3) J. R. Dickinson, S. B. Piepho, J. A. Spencer, and P. N. Schatz, *J. Chem. Phys.*, **56**, 2668 (1972).
(4) S. B. Piepho, J. R. Dickinson, J. A. Spencer, and P. N. Schatz, *J. Chem. Phys.*, **57**, 982 (1972).
(5) S. B. Piepho, J. R. Dickinson, J. A. Spencer, and P. N. Schatz, *Mol. Phys.*, **24**, 609 (1972).
(6) W. H. Inskeep, R. W. Schwartz, and P. N. Schatz, *Mol. Phys.*, **25**, 805 (1973).
(7) P. N. Schatz, "Electronic States of Inorganic Compounds", P. Day, Ed., D. Reidel Publishing Co., 1975, pp 223–240.
(8) S. B. Piepho, W. H. Inskeep, P. N. Schatz, W. Preetz, and H. Homborg, *Mol. Phys.*, **30**, 1569 (1975).
(9) G. C. Allen and K. D. Warren, *Struct. Bonding (Berlin)*, **19**, 105 (1974).
(10) G. C. Allen and K. D. Warren, *Coord. Chem. Rev.*, **16**, 227 (1975).
(11) P. J. Stephens, *J. Chem. Phys.*, **44**, 4060 (1966).
(12) W. Preetz and Y. Petros, *Angew. Chem., Int. Ed. Engl.*, **10**, 936 (1971).
(13) A. J. McCaffery, P. N. Schatz, and T. E. Lester, *J. Chem. Phys.*, **50**, 379 (1969).
(14) R. W. G. Wyckoff, "Crystal Structures", 2nd ed, Vol. 3, Interscience, New York, N.Y., 1965, pp 341 and 408.
(15) G. C. Allen, R. Al-Mobarak, G. A. M. El-Sharkawy, and K. D. Warren, *Inorg. Chem.*, **11**, 787 (1972).
(16) In our discussion of the MCD spectra of OsF_6^{2-} and IrF_6^{2-}, there will be frequent reference to the Faraday $\mathcal{A}$, $\mathcal{B}$, and $\mathcal{C}$ terms, and to the dipole strength, $\mathcal{D}$. We use these symbols without subscript in a generic sense and append subscripts to designate explicit mathematical expressions. We follow the new conventions outlined by Stephens (ref 2a, especially Appendix II). The specific parameters of interest are ^{2a} $\mathcal{A}_1$, $\mathcal{B}_0$, $\mathcal{C}_0$, $\mathcal{D}_0$ which are related to our previous parameters (ref 8) as follows: $\mathcal{D}_0 = D/3$, $\mathcal{A}_1 = 2A/3\beta$, $\mathcal{B}_0 = -2B/3\beta$, $\mathcal{C}_0 = -2C/3\beta$. $\mathcal{A}_1$ is associated with a first-derivative MCD line shape and is *defined* to be positive (negative) if the line shape goes first negative (positive) and then positive (negative) going to higher energy. $\mathcal{B}_0$ and $\mathcal{C}_0$ are associated with absorption-like line shapes and are *defined* as positive (negative) if their accompanying MCD is positive (negative). $\mathcal{D}_0$ is proportional to the (zero-field) absorption band area, $\int(\epsilon/\nu)\,d\nu$. The specific definitions and physical significance of these parameters have been discussed elsewhere.[2a]
(17) (a) P. C. Jordan, H. H. Patterson, and P. B. Dorain, *J. Chem. Phys.*, **49**, 3858 (1968); (b) P. B. Dorain, H. H. Patterson, and P. C. Jordan, *ibid.*, **49**, 3845 (1968).
(18) Throughout, the conventions and notation used are those of J. S. Griffith, "The Theory of Transition-Metal Ions", Cambridge University Press, 1961.
(19) J. S. Griffith, "The Irreducible Tensor Method for Molecular Symmetry Groups", Prentice-Hall, Englewood Cliffs, N.J., 1962.
(20) P. A. Dobosh, *Phys. Rev. A*, **5**, 2376 (1972).
(21) P. A. Dobosh, *Mol. Phys.*, **27**, 689 (1974).
(22) T. A. Keiderling, P. J. Stephens, S. B. Piepho, J. L. Slater, and P. N. Schatz, *Chem. Phys.*, **11**, 343 (1975).
(23) J. C. Collingwood, P. N. Schatz, and P. J. McCarthy, *Mol. Phys.*, **30**, 469 (1975).
(24) C. K. Luk, W. C. Yeakel, F. S. Richardson, and P. N. Schatz, *Chem. Phys. Lett.*, **34**, 147 (1975).
(25) W. C. Yeakel and P. N. Schatz, *J. Chem. Phys.*, **61**, 441 (1974), eq 1.
(26) M. A. Hepworth, P. L. Robinson and G. J. Westland, *J. Chem. Soc.*, 611 (1958).
(27) D. H. Brown, D. R. Russell, and D. W. A. Sharp, *J. Chem. Soc. A*, 18 (1966).
(28) R. D. Peacock and D. W. A. Sharp, *J. Chem. Soc.*, 2762 (1959).
(29) I. N. Douglas, *J. Chem. Phys.*, **51**, 3066 (1969).
(30) A. B. P. Lever, "Inorganic Electronic Spectroscopy", Elsevier, Amsterdam, 1968, p 207.
(31) T. M. Dunn, D. S. McClure, and R. G. Pearson, "Some Aspects of Crystal Field Theory", Harper and Row, New York, N.Y., 1965, p 92.
(32) H. H. Patterson, W. J. De Berry, J. E. Byrne, M. T. Hsu, and J. A. Lo Menzo, *Inorg. Chem.*, **16**, 1698 (1977).

Contribution from the Research Laboratory of Resources Utilization, Tokyo Institute of Technology, Nagatsuta, Midori-ku, Yokohama, Japan

Electronic Raman Spectra of Hexahalogenoosmate(IV) Ions in the Resonant Condition

KEN-ICHI IKEDA and SHIRO MAEDA*

Received April 27, 1978

Electronic Raman spectra of OsX_6^{2-} (X = Cl, Br, and I) ions were obtained in aqueous solutions and were assigned to the T_{1g}, T_{2g}, and E_g spin–orbit levels derived from the lowest $^3T_{1g}$ term of Os(IV). Striking resonance effect was observed for $OsBr_6^{2-}$ which has intense absorption bands in the region of Ar^+ laser lines. The $OsBr_6^{2-}$ spectrum in a low-temperature solid showed some structures assignable to vibroelectronic Raman transitions.

Introduction

In recent years, there has been considerable interest in the Raman spectroscopic investigation of low-lying electronic states of rare earth and transition-metal ions.[1-10] Since the electronic Raman scattering is usually extremely diffused at room temperature, the reported spectra were mostly observed for low-temperature crystalline samples, and few attempts have been made to investigate the resonance Raman effect, which has been a matter of great concern in recent vibrational spectroscopy. In the preceding paper,[11] we reported the observation of a resonance Raman spectrum associated with the low-lying spin–orbit states of $OsBr_6^{2-}$ in aqueous acid solution. The observed electronic Raman lines were extremely broad as expected, showing the widths more than 10 times broader than the vibrational ones, but the scattered intensity was great enough to be clearly measured at room temperature owing to the resonance enhancement. In the present paper, we report the result of further investigation on $OsBr_6^{2-}$ in solution as well as in solid at 77 K, along with the essentially similar but less strikingly resonant spectra of $OsCl_6^{2-}$ and OsI_6^{2-}.

Experimental Section

K_2OsX_6 (X = Cl, Br, and I) was prepared from OsO_4, HX, and KX according to the methods of Turner et al.[12] and Fenn et al.[13] The solution spectra were measured by 1 M HX solutions of K_2OsX_6 for $OsCl_6^{2-}$ and $OsBr_6^{2-}$, but rather unstable K_2OsI_6 was dissolved in a 2 M $HClO_4$ solution saturated with KI to avoid decomposition during the spectral observation. A rotating cell was used throughout the solution measurements. The low-temperature spectra of $OsBr_6^{2-}$ were obtained for the solid formed by quenching the above acid solution with liquid nitrogen. Details of the spectroscopic measurements were the same as reported before, except that a He–Cd laser and a CW dye laser (Rhodamine 6G) were additionally employed for excitation and that the photomultiplier was replaced by the one (HTV R 649) with a higher sensitivity in the long wave region.

0020-1669/78/1317-2698$01.00/0